Design considerations for a highly segmented mirror

Stephen Padin

Design issues for a 30-m highly segmented mirror are explored, with emphasis on parametric models of simple, inexpensive segments. A mirror with many small segments offers cost savings through quantity production and permits high-order active and adaptive wave-front corrections. For a 30-m $f/1.5$ paraboloidal mirror made of spherical, hexagonal glass segments, with simple warping harnesses and three-point supports, the maximum segment diameter is ~100 mm, and the minimum segment thickness is ~5 mm. Large-amplitude, low-order gravitational deformations in the mirror cell can be compensated if the segments are mounted on a plate floating on astatic supports. Because gravitational deformations in the plate are small, the segment actuators require a stroke of only a few tens of micrometers, and the segment positions can be measured by a wave-front sensor. © 2003 Optical Society of America

OCIS codes: 350.1260, 010.1080, 220.4880, 120.4640.

1. Introduction

Multiple mirrors seem to be the only viable approach for optical telescopes with apertures much larger than ~8 m. Many designs have been proposed, and these are broadly distinguished by the size of the subapertures. The 20–20 telescope elements, which have seven 8.4-m-diameter segments,[1] and the Phased Array Mirror Extendible Large Aperture (PAMELA), with 8-cm-diameter segments,[2–4] represent the extremes of the design space. The Keck telescopes, with 1.8-m-diameter segments,[5] and the Hobby-Eberly Telescope, with 1.15-m-diameter segments,[6,7] are the only working multiple-mirror telescopes.

Small segments have potential for a lightweight, low-cost telescope mirror and can support adaptive optics (AO) if the segment diameter is approximately half of the Fried parameter.[8] PAMELA addressed some of these issues, using a scaled version of the Keck approach with inductive edge sensors and voice coil actuators, but the large number of edge sensors and high actuator power consumption make the design unattractive for a very large mirror. Simpler small-segment schemes are possible, and some of the design considerations are explored here for a 30-m $f/1.5$ visible and infrared telescope with AO.

For a large mirror with small segments, the cost and complexity of sensors and actuators are key issues. If gradients in the telescope structural deformations are repeatable at the level of ~1 μm across a segment diameter, changes in the segment positions can be measured by a wave-front sensor instead of edge sensors. The wave-front sensor could also be shared by a high-order AO system. If segment-to-segment piston errors are not repeatable at the level of approximately half of the wave-front sensor wavelength, an iterative piston-stepping algorithm,[9] or measurements at multiple wavelengths, must be used to resolve 2π phase ambiguities. The deformation gradient constraint is severe, but feasible: Axial gravitational deformation of the primary in the 30-m California Extremely Large Telescope (CELT) design is ~10-mm p.-p., i.e., ~700-μm p.-p. on 1-m scales[10]; gravitational deformations in the Keck telescopes are repeatable at the level of 1 part per 1000, so the nonrepeatable deformation in the CELT primary should be <1-μm p.-p. on 1-m scales. A thin highly segmented mirror will have low mass, which will help to achieve small, repeatable structural deformations. Small gravitational deformations on the scale of a segment diameter also allow the mirror to be constructed with small gaps between segments. This is important because it gives a low infrared background and low diffraction pattern sidelobes.

The stroke of the segment actuators is set by gravitational deformations in the telescope structure, but these are mainly on large spatial scales, so it is not efficient for the segments to have expensive, long-

The author is with the California Institute of Technology, Mail Stop 105-24, 1200 East California Boulevard, Pasadena, California 91125. His e-mail address is spadin@caltech.edu.

Received 26 July 2002; revised manuscript received 16 December 2002.

0003-6935/03/163305-08$15.00/0

stroke actuators. An obvious development is a hierarchy of actuators, with a few long-stroke actuators compensating most of the structural deformation and short-stroke actuators on each segment providing fast and small spatial scale wave-front control. This scheme is particularly appropriate if the mirror is made of several rafts of segments because the low-order deformations can be compensated by use of actuators on each raft.[3] Compensation of low-order deformations could also be moved to a fairly small active mirror at an image of the primary, leaving just high-order corrections in the primary. Several different optical designs are possible,[11–14] but the schemes with good image quality have two or three additional reflections that cause a significant sensitivity degradation for long-wavelength infrared observations.[15] A third option, explored in more detail in this paper, is to mount the small segments on a plate floating in a force field, as in a monolithic mirror mount (Ref. 16 and references therein). The plate supports provide axial and radial forces to compensate gravity, so the plate is essentially free of gravitational deformations. This is analogous to a scheme with raft actuators, but the control requirements are simpler because the plate supports can all exert the same elevation-dependent force. The segment actuators can be fairly inexpensive, short-stroke electrostrictive devices.[17] These are fast enough for AO and have low hysteresis so they can be operated without local feedback from sensors on the segments.

The following sections contain an overview of design issues for a mirror with many small segments mounted on a floating plate. The material is in three parts: design of the floating plate; parametric modeling of a simple, inexpensive segment (which is the emphasis of this paper); and optical alignment and AO issues.

2. Floating Mirror Plate

The classical flotation support for a monolithic mirror can be applied to compensate structural deformations in a segmented mirror telescope. In this scheme, the segments are mounted on a plate floating in an astatic, gravity-compensating force field. The shape of the plate is determined only by the support forces and is independent of deformations in the telescope structure. This is an important advantage because the stiffness requirements for the structure can be relaxed. The plate is stiff on small spatial scales, and this helps to minimize piston errors between segments. Segment motions that are due to gravity are also small, so the gaps between segments are set mainly by manufacturing tolerances. This may give a lower infrared background than a mirror with much larger segments mounted in an uncompensated cell.

The mirror plate could be a space-frame structure, or a box with cells made of steel or fiber-reinforced composite sheets. A space frame or box with a stiff face sheet is attractive because it reduces deformations on small scales and provides a convenient interface between the dense array of segment actuators and the more sparse array of mirror plate cells. Because the mirror plate has a simple force-based support, the number of support points can be large, and the plate can then be a fairly thin, lightweight structure.

The floating mirror plate averages segment actuator reaction forces over large spatial scales, and the force-based support decouples the mirror plate from the telescope structure. These effects minimize control–structure interaction for adaptive corrections, so the segments do not require reaction masses, and this helps to reduce the cost and mass of the mirror. The mirror plate is tightly coupled to the segment actuators, and keeping the natural frequencies of the plate modes above the frequencies of adaptive corrections is an important constraint on the plate design. The fundamental frequency of the plate is $f_1 \sim (1/2\pi)(K_1/m_1)^{1/2}$, where $K_1 \propto t_1{}^3/R_1{}^2$ is the stiffness of the plate[18]; and $m_1 = \pi R_1{}^2 t_1 \rho$, t_1, R_1, and ρ are the mass, thickness, radius, and density of the plate, respectively. Thus $f_1 \propto t_1/R_1{}^2$. Modes with Zernike radial degree n have features with a scale size of $\sim R_1/n$, so the natural frequency for modes in the nth radial degree is $f_1(n) \propto n^2$. Adaptive corrections must be made on the time scale of the wind-crossing time for a mode feature, so the frequency for corrections in the nth radial degree is $f_{\mathrm{AO}}(n) \sim un/R_1$, where u is the wind speed. Because $f_1(n)/f_{\mathrm{AO}}(n) \propto n$, a mirror plate that is not excited by the lowest-order adaptive corrections will not be excited by higher-order corrections if the coupling between different mirror plate modes is small. For a 30-m telescope, and a wind speed of 30 ms^{-1} in the turbulent atmospheric layers, the frequency of the lowest-order adaptive corrections is $\sim$2 Hz, so the floating mirror plate should have a fundamental frequency of at least a few hertz. This requires an $\sim$1-m-thick steel box-style mirror plate (see Fig. 1).

The force-based support of the floating mirror plate offers no resistance to wind buffeting, but wind-induced deformations in the mirror can be corrected if they are smaller than the stroke of the segment actuators. Position-based support can be applied on short time scales to provide wind resistance, but at the expense of a lower fundamental frequency for the plate and increased coupling to the telescope structure. If the mirror plate is supported by hydraulic actuators, the cylinders can be connected to an accumulator with small orifices to restrict the hydraulic fluid flow. This couples the mirror plate to the telescope structure on short time scales, and the structure provides stiffness. On long time scales, fluid can flow freely in and out of the cylinders, and the system behaves like a constant force support. The mirror plate control is simple with force actuators, but position actuators can be used if they are fitted with load cells to measure the forces applied to the plate. Hydraulic and pneumatic actuators are particularly appropriate, because many actuators can be connected to a single reservoir to provide constant pressure over the entire mirror plate.

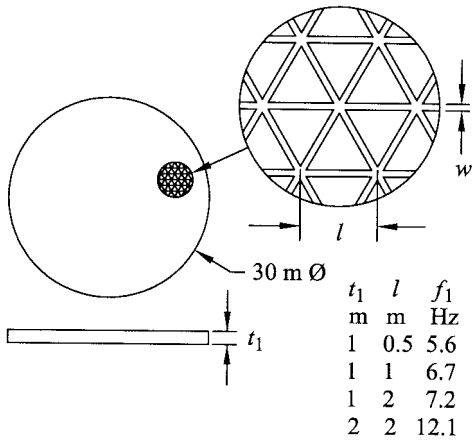

Fig. 1. Fundamental frequencies for several 30-m-diameter box-style floating mirror plates made of steel. The results are from a finite-element model with rectangular plates for the cell walls and triangular plates for the front and back face sheets. For a mirror plate without face sheets, $K_1 \propto wt_1^3/l$ and $m_1 \propto wt_1/l$, where K_1 and m_1 are the stiffness and mass of the mirror plate; hence the fundamental frequency $f_1 \sim (1/2\pi)(K_1/m_1)^{1/2} \propto t_1$ is independent of w and l. The small increase in f_1 with l in the finite-element model is the result of use of single ideal plates for the cell surfaces.

3. Segment Design

In a highly segmented mirror, the segments must achieve adequate optical performance with a simple, inexpensive design. This suggests use of spherical surfaces, warping harnesses, and simple three-point supports. The key performance metric for the mirror is the surface error, which has contributions from figure errors, gravitational deformation, warping harness print-through, actuator position errors, and support-point torques. The latter are caused by bending of the segment supports because of gravity, temperature changes, and actuator operation. Segment design constraints are explored in this section with simple parametric and finite-element models. The initial design of a segment mirror assumes an ideal support; surface errors that are due to support-point torques are included at the end of the section.

The required segment profile, in cylindrical polar coordinates (r, θ, z) centered on the segment, with z normal to the segment surface, is

$$z(r, \theta) \approx z_{\text{focus}} + z_{\text{astig}} + z_{\text{coma}} \approx (2r^2 - 1)\left(\frac{R^2}{4k_1} + \frac{bR^2\zeta^2}{4k_1^3}\right) + (r^2 \cos 2\theta) \times \left(\frac{bR^2\zeta^2}{4k_1^3}\right) + [(3r^2 - 2r)\cos\theta]\left(\frac{bR^3\zeta}{6k_1^3}\right), \quad (1)$$

where r is the segment radial coordinate, normalized to the segment radius R; ζ is the distance of the segment center from the axis of the mirror, and k_1 and b are the radius of curvature and conic constant of the mirror.[19] For a spherical segment, the surface profile is

$$z_s(r, \theta) = (2r^2 - 1)\left(\frac{R^2}{4k} + \frac{R^4}{16k^3} + \frac{R^6}{32k^5} + \dots\right) + r\tau \cos\theta, \quad (2)$$

where k is the radius of curvature of the segment and τ is a tilt in the $(z, \theta = 0)$ plane. In a highly segmented mirror, $R \ll k$, and only the lowest-order terms are significant. A spherical mirror ($b = 0$) is easily synthesized from spherical segments, but for a paraboloidal mirror ($b = -1$) we must warp the segments and adjust k and τ to minimize $z - z_s$. In fairly slow systems with small segments, z_{coma} is negligible (e.g., a 100-mm-diameter segment at the edge of a 30-m $f/1.5$ paraboloid has $z_{\text{coma}} = 0.3$-nm p.-p.).

High-order segment figure errors <25-nm p.-p. ($\lambda/20$ at $\lambda = 0.5$ μm) are reasonable for small, fairly inexpensive optics. Low-order segment figure errors are dominated by the error in the segment radius of curvature, but this can be at least partially corrected by a simple warping harness.[5,20] If the p.-p. manufacturing error in the radius of curvature is 1%, and the error in warping the segments is 10% of the maximum warp, i.e., 0.1% of the radius of curvature, the corresponding figure error is $10^{-3}R^2/2k$ p.-p. For a small, slow segment, a 1% radius of curvature error represents a fairly tight manufacturing tolerance; e.g., with $R = 50$ mm and $k = 90$ m, a 1% error in k corresponds to a segment sagitta error of just 139 nm. Astigmatism can also be compensated with a warping harness (see Fig. 2), and in this case errors in both the orientation and the depth of the warp are important. An error $\Delta\theta$ in the orientation of the warp gives a p.-p. figure error $|b|R^2\zeta^2\Delta\theta/k_1^3$ for $\Delta\theta \ll 1$, and a fractional error $\Delta F/F$ in the warping force gives a p.-p. figure error $(\Delta F/F)|b|R^2\zeta^2/2k_1^3$. For $[(\Delta F/F)^2 + (2\Delta\theta)^2]^{1/2} = 0.1$, i.e., 10% amplitude or 3° orientation error in the warp, the total p.-p. segment figure error is

$$d_{\text{fig}} \approx [(0.1bR^2\zeta^2/2k_1^3)^2 + (10^{-3}R^2/2k)^2 + (25\ \text{nm})^2]^{1/2}. \quad (3)$$

The p.-p. gravitational deformation for a segment on a three-point support is

$$d_{\text{grav}} \approx 0.003\,\frac{mg\pi R^2}{D} = 0.036\,\frac{R^4}{t^2}\,\frac{\pi^2 g\rho(1 - \nu^2)}{E}, \quad (4)$$

where m is the mass of the segment; t is the segment thickness; g is the acceleration that is due to gravity; $D = Et^3/12(1 - \nu^2)$ is the flexural rigidity of the segment; and ρ, ν, and E are the density, Poisson's ratio, and Young's modulus for the segment material, respectively.[21] For a glass segment, with mechanical properties given in Table 1, $d_{\text{grav}} \approx 9.12 \times 10^{-8}R^4/t^2$ p.-p. (d_{grav}, R, and t are in meters).

The warping harness support print-through can be estimated from the pressure required to deflect a plate through a distance equal to the depth of the

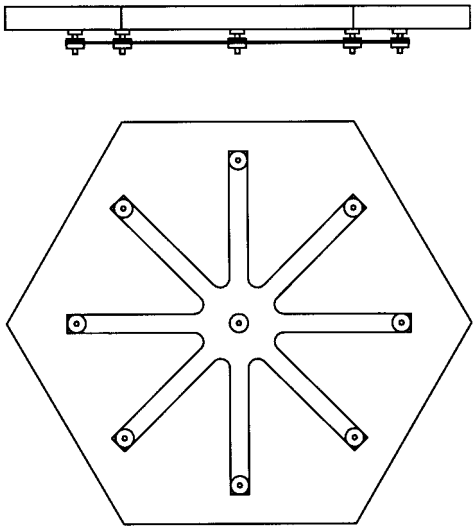

Fig. 2. Nine-point warping harness. This provides a radius of curvature adjustment and a variable-orientation astigmatic warp. The warping spring is clamped to the center of the back of the segment, and the spring arms engage slotted nuts on studs attached to the segment. The slotted nuts are adjusted to set the required figure. If the warping spring is made of steel and the segment is made of glass, a change in temperature will cause a surface error $\sim\xi_{\text{temp}}$ (see Section 3). This effect could be reduced if the warping spring is made from a fiber-reinforced composite with a low thermal-expansion coefficient.

warp. For a change in radius of curvature, the warping harness must support the segment at three points, and the support print-through is $d_{\text{focus}} \approx 0.003q(\pi R^2)^2/D$, where q is the applied pressure [see approximation (4)]. The deflection of a simply supported plate is $\delta = qR^4(5 + \nu)/64(1 + \nu)D$,[18] and a change in radius of curvature Δk changes the segment depth by $\delta = (R^2/2k)(\Delta k/k)$, so the p.-p. support print-through is

$$d_{\text{focus}} \approx 0.003 \frac{R^2}{2k} \frac{\Delta k}{k} \left(\frac{1 + \nu}{5 + \nu}\right) 64\pi^2. \qquad (5)$$

For a glass segment in a 30-m $f/1.5$ mirror, and $\Delta k/k = 0.005$, $d_{\text{focus}} \approx 1.24 \times 10^{-5}R^2$ (d_{focus} and R are in meters). An astigmatic warp requires forces at four points, and the print-through is a factor 3 smaller than for a three-point support. With a change in segment depth equal to the amplitude of z_{astig}, the p.-p. print-through is

$$d_{\text{astig}} \approx 0.001 \frac{|b|R^2\zeta^2}{4{k_1}^3} \left(\frac{1 + \nu}{5 + \nu}\right) 64\pi^2. \qquad (6)$$

Table 1. Material Properties

Property	Glass Ceramic	Stainless Steel	Units
Young's modulus	9.0×10^{10}	2.0×10^{11}	N m^{-2}
Poisson's ratio	0.24	0.30	
Density	2.53×10^{3}	7.85×10^{3}	kg m^{-3}
Thermal-expansion coefficient	10^{-7}	10^{-5}	K^{-1}

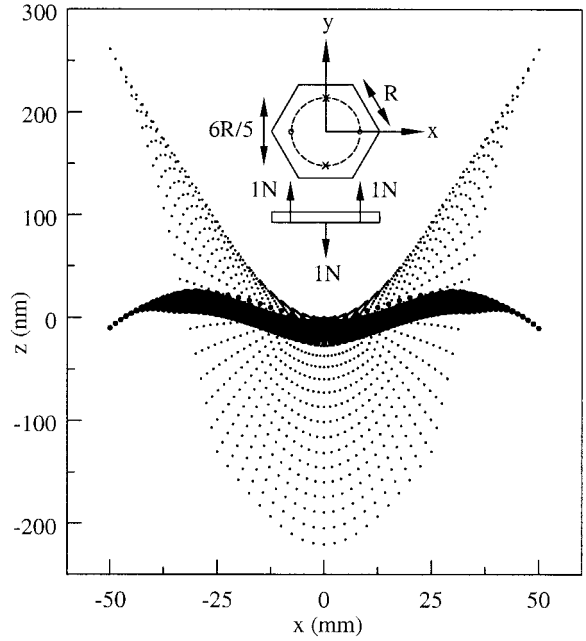

Fig. 3. Finite-element analysis of a 100-mm-diameter, 5-mm-thick hexagonal glass segment in a four-point astigmatic warping harness. The mechanical properties of the segment material are given in Table 1. The small black dots show the deflection of 2400 points across the segment surface, and the large black dots show the residuals (51.8-nm p.-p.) after we fit $z = -0.4 - 8.0(2r^2 - 1) + 283.0r^2 \cos(2\theta)$ nm. For a 100-mm-diameter segment at the edge of a 30-m $f/1.5$ paraboloid, $z_{\text{astig}} = 190r^2 \cos(2\theta)$ nm [approximation (1)]. This requires 0.67 N at each point in the warping harness, and the residual surface profile error is 34.8-nm p.-p., i.e., $d_{\text{astig}} = 1.39 \times 10^{-5}R^2$ (d_{astig} and R are in meters).

For a glass segment at the edge of a 30-m $f/1.5$ paraboloid, $d_{\text{astig}} \approx 1.15 \times 10^{-5}R^2$ (d_{astig} and R are in meters). A finite-element analysis gives $d_{\text{astig}} = 1.39 \times 10^{-5}R^2$ (see Fig. 3), which is close to the value from the plate model. The total support print-through for a glass segment with 1% p.-p. manufacturing error in the radius of curvature, at the edge of a 30-m $f/1.5$ paraboloid, is $d_{\text{warp}} = ({d_{\text{focus}}}^2 + {d_{\text{astig}}}^2)^{1/2} \approx 1.69 \times 10^{-5}R^2$ p.-p. (d_{warp} and R are in meters).

The segment actuator stroke s must be large enough to accommodate uncompensated deformations of a few micrometers in the floating mirror plate, segment mounting errors of a few micrometers (see Section 4), and atmospheric path-length variations if the mirror is used for AO. For Kolmogorov turbulence, the wave-front variance, excluding the piston mode, is $\langle\varphi^2\rangle = 1.03(D_1/r_0)^{5/3}$ rad^2, where D_1 is the diameter of the mirror and r_0 is the Fried parameter.[8,22] A correction range of five times the rms path-length variation requires $s > (D_1/r_0)^{5/6}5\lambda/4\pi$; and at a good site, $r_0(\text{m}) \sim 0.2[2\lambda(\mu\text{m})]^{6/5}$,[23] so $s(\mu\text{m}) > 13[D_1(\text{m})/30]^{5/6}$. The tip–tilt part of the wave-front error can be corrected by a separate fast-steering mirror, so $s \sim 20$ μm should be adequate for both AO and segment position error corrections for a 30-m telescope. Electrostrictive actuators with position feedback only from a wave-front sensor make

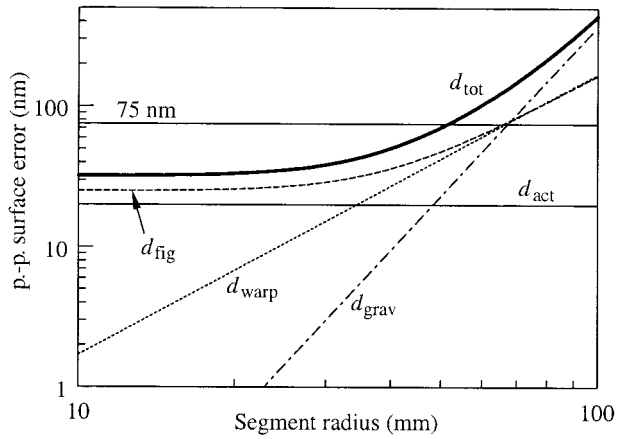

Fig. 4. Surface error contributions for a 5-mm-thick glass segment at the edge of a 30-m $f/1.5$ paraboloid. d_{fig} [approximation (3)] is the segment figure error, when we assume 0.1% error in the radius of curvature, 10% amplitude or 3° orientation error in astigmatism, and 25-nm p.-p. high-order errors; d_{grav} [approximation (4)] is the gravitational deformation of the segment on a three-point support; d_{warp} [quadrature sum of approximations (5) and (6)] is the support print-through when the segment is warped to change the radius of curvature by 0.50% and compensate astigmatism; d_{act} is the segment position error that is due to hysteresis in the segment actuators (1% of a 2-μm step); and d_{tot} is the quadrature sum of all the error contributions. The horizontal line at 75-nm p.-p. surface error corresponds to a 30-nm rms wave-front error.

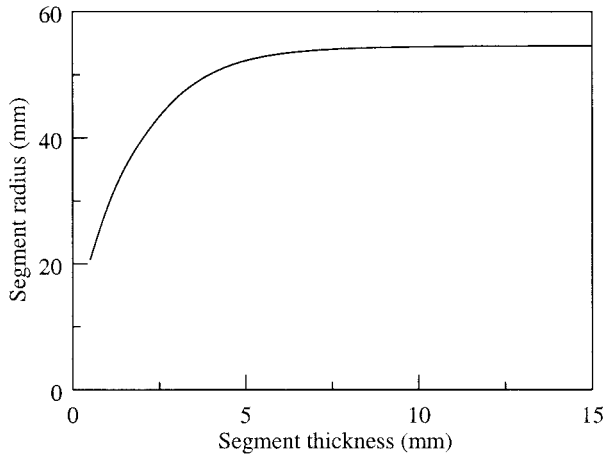

Fig. 5. Segment radius as a function of thickness for a 75-nm p.-p. total surface error.

the segment simple, but at the expense of position errors that are due to actuator hysteresis. This is a small effect for closed-loop operation because the actuators in a high-order AO system do not move much in the wave-front sensor integration time. A position error of 2 μm times the fractional hysteresis is used here as a rough estimate. For electrostrictive materials, the hysteresis is $\sim 0.01s$,[17] so the segment position error is $d_{act} \sim$ 20-nm p.-p.

For an ideal torque-free support, the p.-p. segment surface error is $d_{tot} = (d_{fig}^2 + d_{grav}^2 + d_{warp}^2 + d_{act}^2)^{1/2}$. This is shown in Fig. 4 for a 5-mm-thick glass segment at the edge of a 30-m $f/1.5$ paraboloid. For a wave-front error <30-nm rms, the surface error must be <75-nm p.-p., which requires $R \leq 52$ mm. This is actually an underestimate of the maximum segment radius because d_{fig} and d_{warp} are for a segment at the edge of the mirror (and the worst-case manufacturing error) and d_{grav} is for the full zenith angle range, but most observations are made at zenith angles <70°. Figure 5 shows the segment radius as a function of thickness for d_{tot} = 75-nm p.-p. For thin segments, gravitational deformations dominate, and the segments must be made smaller; but for thick segments, figure errors and warping harness print-through limit the segment radius. The maximum segment radius is ~50 mm, and the corresponding minimum thickness of ~5 mm gives an exceptionally lightweight mirror with a short thermal time constant. A segment diameter of ~100 mm is a good choice for AO at visible wavelengths because $r_0 \sim 200$ mm at $\lambda = 0.5$ μm at a good site. It is also a good choice for extrasolar planet observations because scattering within ~2 arc sec × λ(μm) of the star is controlled by the segment actuators rather than by polishing errors.

A segment must be attached to its actuators with flexures that accommodate changes in temperature and actuator strain. As the flexures bend they apply torques at the segment support points, and the segment deforms. The following deformation estimates are for simple rod flexures of length h and diameter d. Each flexure supports one third of the weight of the segment, so the torque at a segment support point when the telescope is at the horizon is $\tau_{grav} \sim mgh/3$. This corresponds to a force $F_{grav} \sim \tau_{grav}/(R - R_{act})$ at the segment edge, where R_{act} is the radius of the actuator pattern. $R_{act} = R/\sqrt{2}$ for minimum d_{grav}.[24] The torques at the three support points are aligned, so the axial force at the center of the segment is small. The p.-p. segment deformation is

$$\xi_{grav} \sim \frac{2F_{grav}R^2(3+\nu)}{16\pi(1+\nu)D} = \frac{\sqrt{2}R^3\rho gh(3+\nu)(1-\nu)}{2Et^2(\sqrt{2}-1)}, \tag{7}$$

which is a rough estimate based on the deflection of a simply supported segment with force $2F_{grav}$ at the center.[18]

If just one actuator is fully extended, the segment tilts through an angle $\gamma = 2s/3R_{act}$. The flexures bend a distance $\sim h\gamma$, and the torque at each support point is $\sim h^2\gamma K_f$, where $K_f = 3E_fI_f/h^3$ and $I_f = \pi d^4/64$ are the bending stiffness and moment of inertia of a flexure[25] and E_f is Young's modulus for the flexure material. The corresponding p.-p. segment deformation is

$$\xi_{act} \sim \frac{3sE_fd^4(3+\nu)(1-\nu)}{32Et^3h(\sqrt{2}-1)}. \tag{8}$$

A temperature variation ΔT changes the actuator pattern radius and bends the flexures a distance $\alpha R_{act}\Delta T$, where α is the difference between the ex-

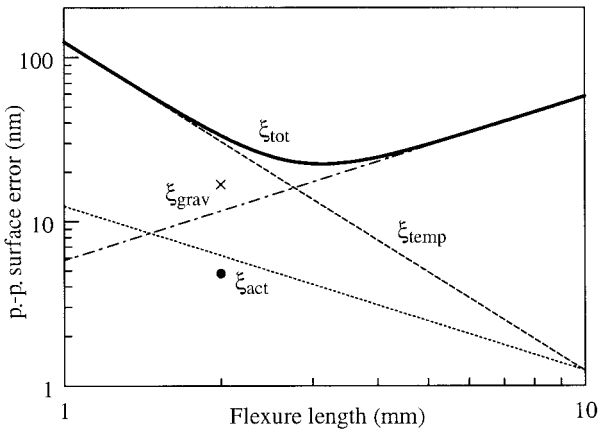

Fig. 6. Surface error that is due to support-point torques for a 100-mm-diameter, 5-mm-thick glass segment on 0.5-mm-diameter steel rod flexures attached to a steel mount. Mechanical properties of the segment and flexure materials are given in Table 1. ξ_{grav} [approximation (7)] is the segment deformation that is due to gravitational deflection of the flexures when the telescope is at the horizon; ξ_{act} [approximation (8)] is the deformation that is due to bending of the flexures when just one actuator is fully extended; ξ_{temp} [approximation (9)] is the deformation that is due to the flexures bending because of a 5 K temperature change; and ξ_{tot} is the quadrature sum of the surface error contributions. The cross and circle are finite-element analysis results for ξ_{grav} and ξ_{act}. ξ_{temp} could be reduced substantially if the segment mount was made from a composite material with a low thermal-expansion coefficient.

pansion coefficients of the segment and its mount. The torque at each support point is $\tau_{temp} = hK_f\alpha R_{act}\Delta T$, which corresponds to a force $\tau_{temp}/(R - R_{act})$ at the segment edge and $-\tau_{temp}/R_{act}$ at the center. The three support-point torques are roughly equivalent to a single force $3\tau_{temp}[1/R_{act} + 1/(R - R_{act})]$ at the center of a simply supported segment. The p.-p. deformation is

$$\xi_{temp} \sim \frac{27R^2E_fd^4\alpha\Delta T(3 + \nu)(1 - \nu)}{128Et^3h^2(2 - \sqrt{2})}. \qquad (9)$$

Both ξ_{act} and ξ_{temp} are proportional to d^4, so it is important to make the flexures thin. Figure 6 shows the segment surface error that is due to support-point torques for a 100-mm-diameter, 5-mm-thick glass segment on 0.5-mm-diameter steel flexures attached to a steel mount. In this case, the optimum flexure length is 3 mm, and the support contributes only ~20-nm p.-p. to the segment surface error.

Figures 4 and 6 suggest that a 30-m $f/1.5$ mirror, with good optical performance, can be made from ~100-mm-diameter spherical segments with warping harnesses and simple three-point supports. This requires $\sim 10^5$ segments, with radius of curvature varying from 90 m on axis to 92.3 m at the edge. For 1% p.-p. manufacturing tolerance on the radius of curvature, three or four different batches, each of a few $\times 10^4$ identical segments, would be required. In a concave mirror, the segment diameter must decrease away from the axis, so each batch would also have a slightly different segment diameter.

For the simple segments in this paper, the fundamental frequency is set by the bending stiffness of the support flexures, so there is a trade-off between the AO bandwidth and the segment surface error that is due to support-point torques. The fundamental frequency is $f \sim (1/2\pi)(3K_f/m)^{1/2}$; and for a 100-mm-diameter, 5-mm-thick glass segment on 0.5-mm-diameter, 2-mm-long steel flexures, $f \sim 420$ Hz. This model tends to underestimate K_f and f because it constrains the flexures at only one end. A finite-element analysis yields $f = 628$ Hz. For a typical wind speed of 30 ms^{-1} in a high turbulent layer, the wind-crossing frequency for a segment radius of 50 mm is 600 Hz, so the simple segment design is just able to support the highest-order AO modes. The response of a segment to wind buffeting is also set by the stiffness of the support flexures, but in this case the axial stiffness is relevant. A 100-mm-diameter segment on 0.5-mm-diameter, 2-mm-long steel flexures has a stiffness of $\sim 7 \times 10^9$ Pa m^{-1}; compare this with $\sim 10^7$ Pa m^{-1} for the 1-m-diameter segments in the CELT.[10] On small spatial scales, a highly segmented mirror can have high stiffness, and hence good wind resistance, because the support-point density is high; on large spatial scales, the stiffness is limited by the floating mirror plate and its support structure (see Section 2).

4. Optical Alignment

An important feature of the mirror design described in this paper is use of only a wave-front sensor to measure the segment positions. This is attractive because the segment control depends directly on the quality of the wave front delivered by the telescope, but the approach is not simple because a large wave-front sensor is required. A mirror with N segments, and three actuators per segment, must have at least $3N/2$ wave-front sensor subapertures to measure all the degrees of freedom. A hexagonal subaperture array with one subaperture per segment edge (i.e., three subapertures per segment) gives the average tilt of the mirror surface at each segment edge and should be enough to calculate all the segment tilts and relative piston errors. Adding a subaperture at the center of each segment fills the array and provides an independent measurement of the tilt of each segment (see Fig. 7). This scheme requires a hexagonal lenslet array with $4N$ elements and a rectangular detector array with an aspect ratio of $\cos(\pi/6)$ and $16N$ pixels (i.e., $\sim 4 \times 10^5$ lenslets and 1.6 million pixels for a 30-m telescope with 100-mm-diameter segments). The wave-front reconstruction for $4N$ subapertures and $3N$ actuators requires $8N \times 3N$ multiply-and-add operations, which is possible for a 1-Hz update rate for active corrections with 10^5 segments, but requires some development for AO.

The wave-front sensor subapertures are small for a highly segmented mirror, so a laser guide star is required. For a Shack–Hartmann sensor measuring all $3N$ modes of the mirror, the wave-front vari-

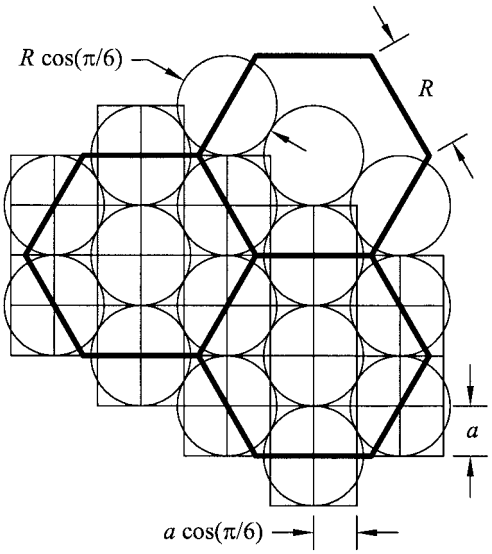

Fig. 7. Wave-front sensor subaperture and detector configuration. The bold hexagons are mirror segments, the circles are wave-front sensor subapertures (1 + 6/2 per segment), and the rectangles represent the assignment of detector pixels to subapertures (four pixels per subaperture if there are no guard bands).

ance in each sensed mode is $\langle\sigma^2\rangle \approx \pi^2/3NpA$ rad^2, where p is the number of photons per unit area incident on the telescope and A is the area of a wave-front sensor subaperture in the entrance pupil.[26] For a hexagonal array of circular subapertures, $A = \pi[R\cos(\pi/6)]^2/4 \approx R^2/2$. The total wave-front variance is then $3N\langle\sigma^2\rangle \approx 2\pi^2/pR^2$ rad^2, and the total path-length variance is $\langle\epsilon^2\rangle = 3N\langle\sigma^2\rangle(\lambda/2\pi)^2 \approx \lambda^2/2pR^2$. At $\lambda = 0.63$ μm, an mth magnitude spectral-type AO star provides $p \sim 2.4 \times 10^{10-0.4m}$ photons m^{-2} in a 1-s integration time and 0.3-μm bandwidth; so for $R = 50$ mm, $m \sim 51.2 + 5\log(\tau_{\text{int}}{}^{1/2}\langle\epsilon^2\rangle^{1/2})$, where τ_{int} is the wave-front sensor integration time in seconds and ϵ is in meters. For $\langle\epsilon^2\rangle^{1/2} = 5$ nm and $\tau_{\text{int}} = 1$ s, $m \sim 9.7$, which requires a laser guide star for most observations.[27] Gravitational and thermal deformations in the telescope structure vary slowly, so τ_{int} could probably be increased to 10 s for active corrections, which would allow a 12th magnitude guide star.

Because the segment actuators have a short stroke, initial alignment of the segments is an important consideration. Of course the corollary is that, once this problem is solved, the segments can be phased quickly,[9,28] and recovery from a segment change is rapid. During assembly, the radius of curvature and astigmatism of each segment must be set within ~0.1% and ~10%, respectively, and the height of the segment and its mount must be measured with an accuracy of a few micrometers. These measurements and adjustments could be automated. The relative heights of the segment mounting nodes on the telescope must also be measured with an accuracy of a few micrometers. This could be done with a laser interferometer mounted on a plate that replaces a segment assembly, with a fixed retroreflector mounted near the secondary. Prior to segment installation, each mounting node must be adjusted to match its segment, based on the segment height and node height measurements. Installing 10^5 segments is a substantial task that would require parallel operations and automated tracking of all the measurements.

5. Discussion

The maintenance of a highly segmented mirror is an important consideration because mirror coatings have a finite lifetime. Mounting the segments on rafts allows them to be replaced in batches, but this approach breaks up the mirror support structure and encourages piston errors at raft boundaries. If the segments have a simple release mechanism, they could be handled one at a time, perhaps by a robot. An important advantage of small segments is that multilayer coatings can be used to improve the reflectivity and lifetime of the surface.[29–31] This simplifies the logistics of recoating and increases the throughput of the telescope. Small segments also reduce the cost of the recoating facility.

The segment design details given in this paper suggest that a large mirror, with good optical performance, can be made from small spherical segments with warping harnesses. A simple three-point segment support is adequate for both axial and radial loads. Mounting the segments on a floating plate that compensates gravitational deformations allows use of inexpensive, short-stroke segment actuators and can significantly relax the stiffness requirements for the telescope structure. This scheme is also appropriate for AO because it decouples the segment actuators from the structure. AO is an attractive feature of a highly segmented mirror, but the approach also offers real potential for cost savings through quantity production of simple optics.

This research was supported by the Caltech Discovery Fund.

References

1. R. Angel, M. Lloyd-Hart, K. Hedge, R. Sarlot, and C. Peng, "The 20/20 telescope: MCAO imaging at the individual and combined foci," in *Proceedings of ESO Conference on Beyond Conventional Adaptive Optics*, R. Ragazzoni and S. Esposito, eds. (to be published).
2. A. D. Gleckler, D. J. Markason, and G. H. Ames, "PAMELA: control of a segmented mirror via wavefront tilt and segment piston sensing," in *Active and Adaptive Optical Components*, M. A. Ealey, ed., Proc. SPIE **1543,** 176–189 (1991).
3. S. C. Fawcett, "Development of adaptive optical segments with integrated wave front sensing," in *Active and Adaptive Optical Components and Systems II*, M. A. Ealey, ed., Proc. SPIE **1920,** 193–199 (1993).
4. J. M. Rakoczy, E. E. Montgomery, and J. L. Lindner, "Recent enhancements of the Phased Array Mirror Extendible Large Aperture (PAMELA) telescope testbed at MSFC," in *Telescope Structures, Enclosures, Controls, Assembly/Integration/Validation and Commissioning*, T. A. Sebring and T. Anderson, eds., Proc. SPIE **4004,** 352–362 (2000).
5. J. E. Nelson, T. S. Mast, and S. M. Faber, eds., "The design of

the Keck Observatory and Telescope," Keck Observatory Rep. 90 (Keck Observatory, Kamuela, Hawaii, 1985).
6. V. L. Krabbendam, T. A. Sebring, F. B. Ray, and J. R. Fowler, "Development and performance of Hobby-Eberly Telescope 11-m segmented mirror," in *Advanced Technology Optical/IR Telescopes VI*, L. M. Stepp, ed., Proc. SPIE **3352,** 436–445 (1998).
7. L. W. Ramsey, M. T. Adams, T. G. Barnes, J. A. Booth, M. E. Cornell, J. R. Fowler, N. Gaffney, J. W. Glaspey, J. Good, G. J. Hill, P. W. Kelton, V. L. Krabbendam, L. Long, P. J. MacQueen, F. B. Ray, R. L. Ricklefs, J. Sage, T. A. Sebring, W. J. Spiesman, and M. Steiner, "The early performance and present status of the Hobby-Eberly Telescope," in *Advanced Technology Optical/IR Telescopes VI*, L. M. Stepp, ed., Proc. SPIE **3352,** 34–42 (1998).
8. D. L. Fried, "Statistics of a geometric representation of wavefront distortion," J. Opt. Soc. Am. **55,** 1427–1435 (1965).
9. G. Chanan, M. Troy, F. Dekens, S. Michaels, J. Nelson, T. Mast, and D. Kirkman, "Phasing the mirror segments of the Keck telescopes: the broadband phasing algorithm," Appl. Opt. **37,** 140–155 (1998).
10. J. E. Nelson and T. S. Mast, eds., "Conceptual design for a thirty-meter telescope," CELT Rep. 34 (University of California, Santa Cruz, Santa Cruz, Calif., 2002).
11. P.-S. Kildal, L. A. Baker, and T. Hagfors, "The Arecibo upgrading: electrical design and expected performance of the dual-reflector feed system," Proc. IEEE **82,** 714–724 (1994).
12. J. M. Sasian, "Four-mirror optical system for large telescopes," Opt. Eng. **29,** 1181–1185 (1990).
13. D. Korsch, "Closed form solution for three-mirror telescopes, corrected for spherical aberration, coma, astigmatism, and field curvature," Appl. Opt. **11,** 2986–2987 (1972).
14. R. N. Wilson and B. Delabre, "New optical solutions for very large telescopes using a spherical primary," Astron. Astrophys. **294,** 322–338 (1995).
15. M. Lloyd-Hart, "Thermal performance enhancement of adaptive optics by use of a deformable secondary mirror," Publ. Astron. Soc. Pac. **112,** 264–272 (2000).
16. R. N. Wilson, *Reflecting Telescope Optics II* (Springer-Verlag, Berlin, Germany, 1999), Chap. 3.
17. M. Ealey, "Actuators: design fundamentals, key performance specifications, and parametric trades," in *Active and Adaptive Optical Components*, M. A. Ealey, ed., Proc. SPIE **1543,** 346–362 (1991).
18. S. Timoshenko and S. Woinowsky-Krieger, *Theory of Plates and Shells* (McGraw-Hill, New York, 1959), Chap. 3.
19. T. S. Mast, J. E. Nelson, and G. E. Sommargren, "Primary mirror segment fabrication for CELT," in *Optical Design, Materials, Fabrication and Maintenance*, P. Dierickx, ed., Proc. SPIE **4003,** 43–58 (2000).
20. T. S. Mast and J. E. Nelson, "The fabrication of large optical surfaces using a combination of polishing and mirror bending," in *Advanced Technology Optical Telescopes IV*, L. D. Barr, ed., Proc. SPIE **1236,** 670–681 (1990).
21. J. E. Nelson, J. Lubliner, and T. S. Mast, "Telescope mirror supports: plate deflections on point supports," in *Advanced Technology Optical Telescopes*, G. Burbidge and L. D. Barr, eds., Proc. SPIE **332,** 212–228 (1982).
22. R. J. Noll, "Zernike polynomials and atmospheric turbulence," J. Opt. Soc. Am. **66,** 207–211 (1976).
23. F. Roddier, "The effects of atmospheric turbulence in optical astronomy," in *Progress in Optics*, Vol. 19, E. Wolf, ed. (North-Holland, Amsterdam, 1981), pp. 281–376.
24. J. B. Hindle, "Floatation systems," in *Amateur Telescope Making*, A. G. Ingalls, ed., (Munn, 1947), pp. 229–234.
25. J. W. Hardy, *Adaptive Optics for Astronomical Telescopes* (Oxford U. Press, Oxford, UK, 1998), Chap. 6.
26. F. Roddier, ed., *Adaptive Optics in Astronomy* (Cambridge U. Press, Cambridge, UK, 1999), Chap. 3.
27. J. N. Bachall and R. M. Soneira, "The distribution of stars to $V = 16^{th}$ magnitude near the north galactic pole: normalization, clustering properties, and counts in various bands," Astrophys. J. **246,** 122–135 (1981).
28. G. Chanan, M. Troy, and E. Sirko, "Phase discontinuity sensing: a method for phasing segmented mirrors in the infrared," Appl. Opt. **38,** 704–713 (1999).
29. N. Thomas and J. Wolfe, "UV-shifted durable silver coating for astronomical mirrors," in *Optical Design, Materials, Fabrication and Maintenance*, P. Dierickx, ed., Proc. SPIE **4003,** 312–323 (2000).
30. S. D. Browning, M. R. Jacobson, H. A. Macleod, R. H. Potoff, D. J. Song, and F. Van Milligen, "Development of high reflectance coatings for ground-based astronomical instruments," in *Advanced Technology Optical Telescopes*, G. Burbidge and L. D. Barr, eds., Proc. SPIE **332,** 310–314 (1982).
31. D. Y. Song and H. A. Macleod, "Multilayer coatings for astronomical telescope mirrors," in *Southwest Conference on Optics*, S. C. Stotlar, ed., Proc. SPIE **540,** 156–159 (1985).